Bio-Design and Manufacturing (2021) 4:867–878
https://doi.org/10.1007/s42242-021-00151-6

RESEARCH ARTICLE

4D printing of PLA/PCL shape memory composites with controllable sequential deformation

Suqian Ma[1] · Zeyu Jiang[1] · Meng Wang[1] · Lan Zhang[1] · Yunhong Liang[1] · Zhihui Zhang[1] · Lei Ren[1,2] · Luquan Ren[1]

Received: 7 December 2020 / Accepted: 12 June 2021 / Published online: 16 July 2021

Abstract

Shape memory polymers (SMPs) are a promising class of materials for biomedical applications due to their favorable mechanical properties, fast response, and good biocompatibility. However, it is difficult to achieve controllable sequential shape change for most SMPs due to their high deformation temperature and the simplex deformation process. Herein, shape memory composites based on polylactic acid (PLA) matrix and semi-crystalline linear polymer polycaprolactone (PCL) are fabricated using 4D printing technology. Compared with pure PLA, with the rise of PCL content, the 4D-printed PLA/PCL composites show decreased glass transition temperature (T_g) from 67.2 to 55.2 °C. Through the precise control of the deformation condition, controllable sequential deformation with an outstanding shape memory effect can be achieved for the PLA/PCL shape memory composites. The response time of shape recovery is less than 1.2 s, and the shape fixation/recovery rates are above 92%. In order to simulate sequential petal opening and sequential drug releasing effects, a double-layer bionic flower and a drug release device, respectively, are presented by assembling PLA/PCL samples with different PLA/PCL ratios. The results indicate the potential applications of 4D-printed PLA/PCL composites in the field of bio-inspired robotics and biomedical devices.

Graphic abstract

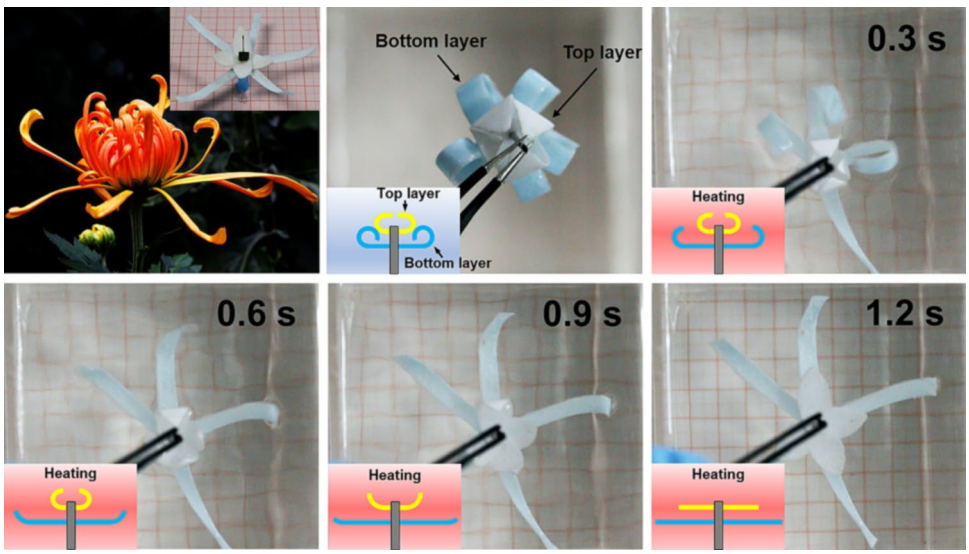

Keywords 4D printing · Shape memory polymer · Temperature-responsive · Polylactic acid · Polycaprolactone

✉ Yunhong Liang
liangyunhong@jlu.edu.cn

[1] The Key Laboratory of Bionic Engineering, Ministry of Education, Jilin University, Changchun 130025, China

[2] Department of Mechanical, Aerospace and Civil Engineering, University of Manchester, Manchester M13 9PL, UK

Introduction

Shape memory polymers (SMPs) are a kind of smart materials that can recover their initial shapes under external stimuli (such as heat, light, electricity, etc.) after going through shape deformation processes [1–4]. Due to the shape memory effect, SMP-based materials have potential applications in the field of biomedical devices and tissue engineering and thus have attracted increasing interest from academic and industrial researchers [5, 6]. However, the development of SMPs still faces certain challenges. One of the most important issues is that, owing to the high glass transition temperature (T_g) of the material of most heat-responsive SMPs, the deformation temperature is too high for application in the biomedical field [7]. One solution to adjust the T_g of the SMPs is to develop SMP composites by adding modifying materials [8]. However, the limitations of traditional processing methods still make it difficult to fabricate desired architectures based on SMP composites.

Three-dimensional (3D) printing, also called additive manufacturing, is emerging as an attractive material manufacturing method, and is based on the principle of printing 3D objects layer-by-layer [9–16]. The concept of "4D printing" was first proposed in the 2013 TED (Technology, Entertainment, Design) Talk, and was defined as "3D printed smart materials" with the fourth dimension being time. Compared with the traditional manufacturing methods, the 4D printing of SMPs has many advantages, such as low cost, simple process, and the realization of fabricating complex structures and composites [17–21]. Ge et al. reported the high-resolution 4D printing of SMP materials, and presented complex structures such as a scale model of the Eiffel Tower and a cardiovascular stent [22]. Wei et al. demonstrated 4D-printed magnetic active SMPs that can be used as remotely actuated self-expandable intravascular stents [23]. However, the 4D printing of SMP composites with decreased T_g and controllable sequential shape change has been scarcely reported.

The direct-write (DW) printing technique is designed to realize the fabrication of various composites from different materials [24]. In this paper, a series of polylactic acid (PLA)/polycaprolactone (PCL) composites were printed from PLA/PCL ink based on DW printing, which was prepared by adding different amounts of semi-crystalline PCL to the shape memory PLA matrix. The influence of PCL concentration on the thermodynamic behaviors, microscopic structures, and mechanical properties was studied by analyzing the different 4D-printed PLA/PCL composites produced. The shape memory effects of the 4D-printed PLA/PCL were further investigated to show the shape memory properties, such as recovery speed, shape fixation rate, and shape recovery rate. Moreover, by assembling PLA/PCL samples with different PLA/PCL ratios, a double-layer bionic flower and a drug release device were fabricated to demonstrate the controllable sequential deformation process, which indicated the potential applications of 4D-printed PLA/PCL composites in the field of bio-inspired robotics and biomedical devices.

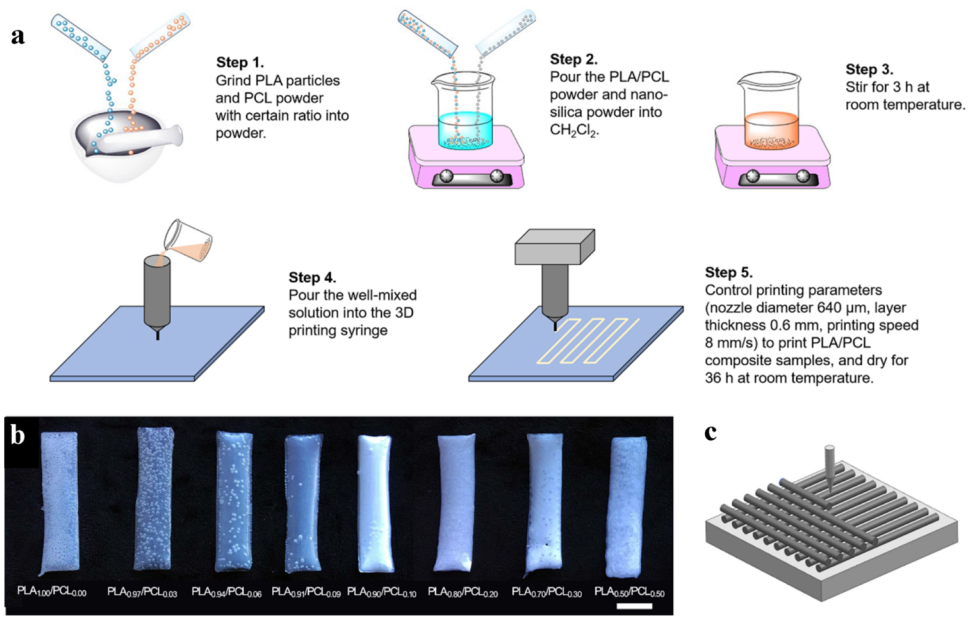

Fig. 1 **a** Schematic illustration of the DW printing process of PLA/PCL composites. **b** Photographs of the 4D-printed PLA/PCL samples. Scale bar: 1 cm. **c** The printing path of the materials

Experiment

Material preparation

The fabrication of PLA/PCL composites includes the processes of ink preparation and the DW 3D printing (Fig. 1a), and its detailed steps are as follows: (1) the PLA particles and PCL powders (non-crosslinked) purchased from Xincheng Engineering Company Ltd. were mixed and ground to form powders well-blended in certain ratios according to Table A1 in Appendix; (2) the PLA/PCL powder and nano-silica (used as a thickener and purchased from Aladdin Reagent Co. Ltd.) were added to CH_2Cl_2 with a mass ratio of PLA/PCL:nano-silica:CH_2Cl_2 = 1:0.0005:3; (3) the mixture was stirred for 3 h at room temperature to obtain a PLA/PCL composite ink with suitable viscosity; (4) the well-mixed PLA/PCL composite ink was poured into a syringe on the homemade DW 3D printer (Fig. A1, see Appendix); (5) according to the sample model created by SolidWorks software, the samples were 3D printed with suitable printing routes that were controlled by the Slic3r software. The nozzle diameter and printing speed were 640 μm and 8 mm/s, respectively. Finally, the printed samples were dried at room temperature for 36 h.

Characterization and measurements

A Fourier transform infrared (FT-IR) spectroscope (IRAffinity-1, Shimadzu, Japan) was used to study the chemical structures of the PLA/PCL composites. The printed samples were ground into powder in a mortar and then mixed with potassium bromide (KBr) powder for testing. The microstructures of the samples were analyzed by scanning electron microscopy (SEM) using the model EVO-18 from Carl Zeiss Company, Germany.

According to the ISO 527-3 standard, the mechanical properties of the 3D-printed samples were detected on a uniaxial tensile testing machine (WDW-500, Weidu Electronics, China) equipped with a 500 N load cell. The size of strip samples was 150 mm × 10 mm × 0.5 mm. All tests were run at a test speed of 0.5 mm/min. Five specimens of each type were tested until failure occurred. For comparison, a pure PLA sample fabricated by molding was also measured.

The differential scanning calorimetry (DSC) experiment was carried out on a DSC-25 instrument from TA Instruments, USA, to investigate the melt crystallization behaviors and glass transition behaviors of the PLA/PCL samples. After keeping the PLA/PCL samples at 25 °C for 10 min, the first heating scan was performed under heating from 25 to 300 °C at a speed of 15 °C/min. Subsequently, the samples were kept at 300 °C for 1 min and cooled down to room temperature at a speed of 5 °C/min to eliminate the thermal stress. The second heating scan was then performed under heating to 300 °C at a speed of 10 °C/min, which was recorded for analysis.

Dynamic mechanical analysis (DMA) was conducted on a SDTA861 DMA instrument, USA, to investigate the thermomechanical properties of the printed samples. The parameters of the experiment were set as a frequency of 1 Hz, an amplitude of 10 μm, and a heating speed of 5 °C /min. After erasing the thermal history at 100 °C for 15 min, DMA tests were performed while heating from 0 to 160 °C at a speed of 5 °C/min. The size of the sample was 15 mm × 7 mm × 0.5 mm.

Shape memory effect

The shape memory behaviors of the fabricated 4D-printed samples were tested by the shape memory cycle method. First, the initial shape of the sample was changed to a temporary shape upon external force at the deformation temperature (i.e., T_g + 20 °C). Next, the sample was cooled down to room temperature to fix the temporary shape. Finally, the sample was heated to the deformation temperature again to demonstrate the shape recovery process. The size of the sample was 45 mm × 10 mm × 0.5 mm.

Results and discussion

Preparation of 4D-printed PLA/PCL composites

The DW printer used here was a homemade equipment depicted in Fig. A1 in Appendix. The PLA particles and PCL powders were purchased and used as received. As a semi-crystalline linear polymer, PCL was added to modify the thermomechanical properties of PLA matrix, which is widely used in the biomedical fields due to its biocompatibility and shape memory effect. For 3D printing, the PLA/PCL composite was prepared into solution state, which had shear thinning properties by the addition of hydrophilic nano-silica as a thickener. To manipulate the thermomechanical and shape memory properties, a series of PLA/PCL composite solution inks with different PCL ratios were prepared according to Table A1 in Appendix. Figure 1a shows the schematic diagram of the fabrication of PLA/PCL composites, and the printing routes are presented in Fig. 1c with parallel paths in each layer and perpendicular paths between layers.

After drying at room temperature, a series of PLA_{1-x}/PCL_x (x is the content of PCL) composites were obtained as shown in Fig. 1b. Herein, the 4D-printed PLA/PCL composites with PCL mass fractions of 0, 3%, 6%, 9%, 10%, 20%,

30%, and 50% were prepared as $PLA_{1.00}/PCL_{0.00}$, $PLA_{0.97}/PCL_{0.03}$, $PLA_{0.94}/PCL_{0.06}$, $PLA_{0.91}/PCL_{0.09}$, $PLA_{0.90}/PCL_{0.10}$, $PLA_{0.80}/PCL_{0.20}$, $PLA_{0.70}/PCL_{0.30}$, and $PLA_{0.50}/PCL_{0.50}$, respectively. The photographs in Fig. 1b obviously show that, with the increase in PCL content, the shapes of the printed samples became more curved. This is because in the DW printing process, the shear stress is generated during the movement of the printing head against the substrate, and will be stored in the PLA/PCL composite materials. In this case, the internal stress will be released from the flexible PCL polymer chains by drying the materials, leading to the recovery of the initial curve state of the printed PLA/PCL composites.

SEM and FT-IR of the samples

The cross-section of microstructures of different 4D-printed PLA/PCL composites was investigated by SEM. As shown in Fig. 2a, for the 4D-printed pure PLA samples ($PLA_{1.00}/PCL_{0.00}$), the morphology is smooth and homogeneous. When adding PCL to PLA matrix (Figs. 2b–2d), PCL appears as microparticles with diameters of about 20 μm, which are uniformly distributed in the PLA matrix. Figure 2b demonstrates that, in $PLA_{0.90}/PCL_{0.10}$ composite, small air gaps are formed around the PCL microparticles, indicating the separation of the PLA matrix and the PCL microparticles. With the increase in PCL content, as shown in the $PLA_{0.50}/PCL_{0.50}$ composite (Fig. 2d), the concentration of the PCL microparticles increases, while the particle size stays unchanged. Therefore, based on the SEM images of the 4D-printed PLA/PCL composites, it is indicated that PCL particles are physically blended in the PLA matrix without chemical reactions, which can also be validated by the FT-IR analysis.

The chemical structures of the 4D-printed PLA/PCL composite samples were measured by an FT-IR spectroscope, with the results shown in Fig. 3a. For pure PLA, the infrared absorption peaks of different functional groups appear at 3430 cm^{-1} (–OH), 1730 cm^{-1} (C = O), 950 cm^{-1} (C–O–C), 1050 cm^{-1} (C–O–C), 1150 cm^{-1} (C–O–C), 2850 cm^{-1} (–CH), 1340 cm^{-1} (–CH), 2960 cm^{-1} ($–CH_3$), and 1450 cm^{-1} ($–CH_3$). For pure PCL, the absorption peaks are 1732 cm^{-1} (C = O), 956 cm^{-1} (C–O–C), 1066 cm^{-1} (C–O–C), 1171 cm^{-1} (C–O–C), 2950 cm^{-1} (–CH), and 1380 cm^{-1} (–CH). The blue curve in Fig. 3a clearly shows that the infrared absorption peaks of the printed $PLA_{0.50}/PCL_{0.50}$ composites comprise the combination of the peaks of pure PLA and PCL. The absence of new characteristic peaks indicates that there are no chemical reactions occurring between PLA and PCL.

Mechanical properties

The mechanical properties of the printed PLA/PCL composites were measured using a uniaxial tensile testing machine, as presented in Fig. 3b. A comparison sample of

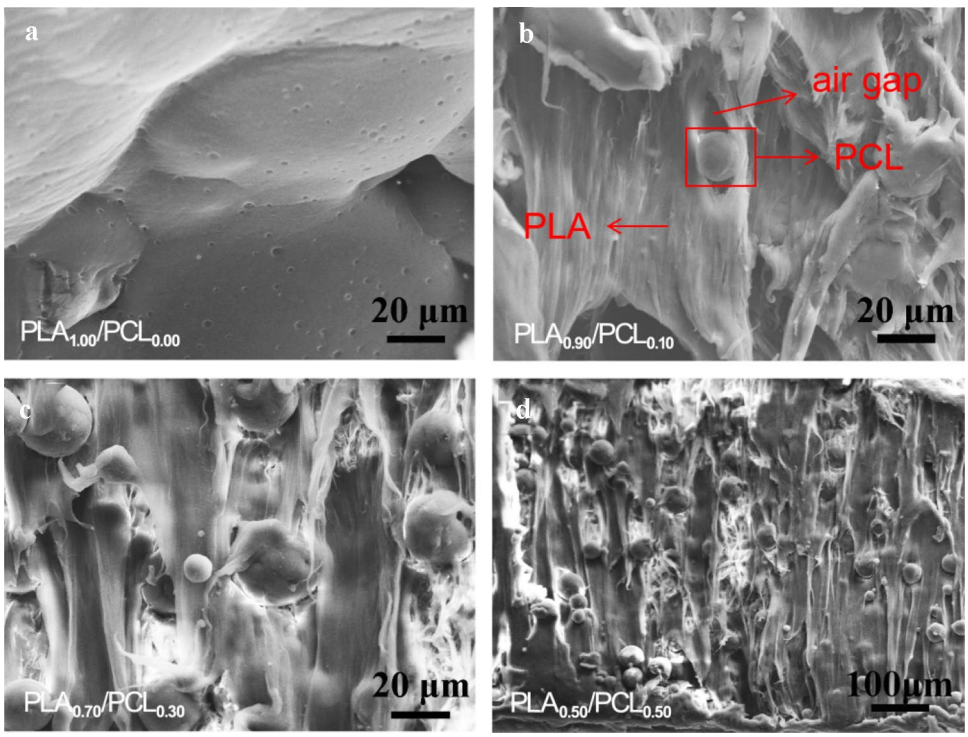

Fig. 2 SEM images of the 4D-printed PLA/PCL composites with different PCL contents. **a** $PLA_{1.00}/PCL_{0.00}$; **b** $PLA_{0.90}/PCL_{0.10}$; **c** $PLA_{0.70}/PCL_{0.30}$; **d** $PLA_{0.50}/PCL_{0.50}$

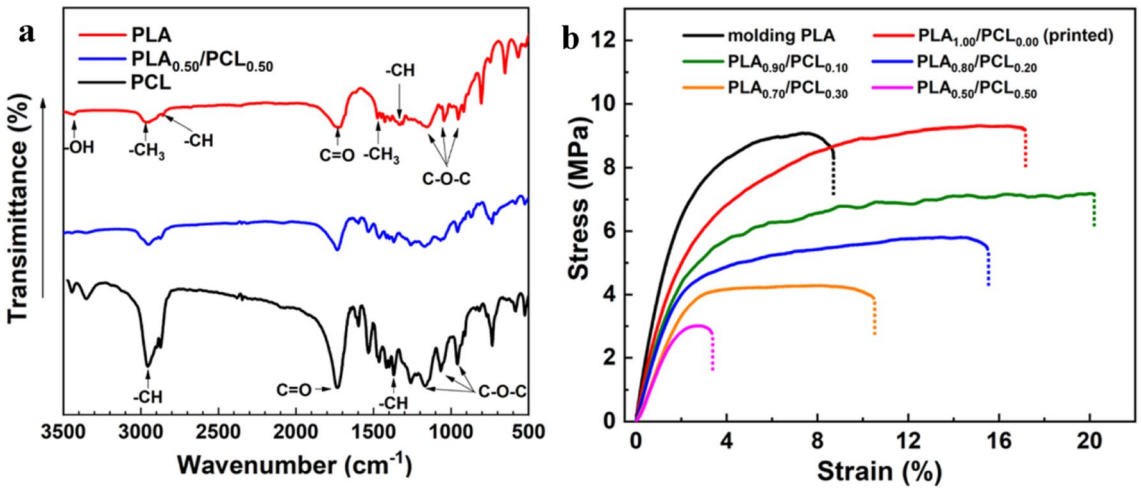

Fig. 3 **a** FT-IR spectra of 4D-printed pure PLA, $PLA_{0.50}/PCL_{0.50}$, and pure PCL. **b** Strain–stress curves of the molded PLA and the 4D-printed PLA_{1-x}/PCL_x composites

Table 1 Maximum stress, strain, and modulus of molded PLA and 4D-printed PLA/PCL composites

Sample	Maximum stress (MPa)	Maximum strain (%)	Modulus (MPa)
Molded PLA	9.07	8.69	471
$PLA_{1.00}/PCL_{0.00}$	9.32	16.86	359
$PLA_{0.90}/PCL_{0.10}$	7.18	20.20	260
$PLA_{0.80}/PCL_{0.20}$	5.80	15.52	251
$PLA_{0.70}/PCL_{0.30}$	4.29	10.51	146
$PLA_{0.50}/PCL_{0.50}$	3.02	3.38	125

pure PLA made by the molding method was prepared using a Teflon mold (Fig. A2, see Appendix). The stress–strain curves and the measurement results in Table 1 show that the molded PLA has a strain of 8.69% at breaking point. As for the 3D-printed PLA, the maximum strain increases significantly to 16.86%, indicating the increased flexibility of PLA when fabricated by 3D printing. Although the modulus of the 3D-printed PLA decreases slightly compared to the molded PLA, the maximum stress of the 3D-printed PLA increases to 9.32 MPa, demonstrating that the DW printing method in this study can maintain the favorable mechanical properties of PLA. By adding 10% of PCL into PLA, the 3D-printed $PLA_{0.90}/PCL_{0.10}$ composites show increased strain of 20.20%, indicating that a small amount of PCL can increase PLA flexibility, which is beneficial for applications in soft actuators. However, when the PCL content is $\geq 20\%$, the maximum strain and the modulus of the printed PLA/PCL composites decrease with increasing PCL content, which might be attributed to the growing number of air gaps and the stress concentration around the PCL microparticles, as shown in the SEM images.

Thermal and dynamic mechanical properties

Besides the mechanical properties, the addition of PCL to the PLA matrix will also affect the thermal properties. The DSC tests were performed for the 4D-printed PLA/PCL composites, and the results are shown in Figs. 4a and 4b. As demonstrated in Fig. 4b, the glass transition temperature (T_g) of the 4D-printed PLA/PCL composites decreases with increasing PCL content. The T_g of $PLA_{0.50}/PCL_{0.50}$ is 55.2 °C, which is 12 °C lower than that of pure PLA (67.2 °C). This is because the semi-crystalline PCL molecular chains can affect the crystallization process of PLA. For most of the thermal-stimuli SMPs, T_g corresponds to the deformation temperature. The decrease in T_g is desirable for SMP materials, since the SMPs used in the biomedical field, such as intravascular stents, are preferred to have deformation temperatures close to 37 °C. The evolution of melting temperatures (T_m) of the 4D-printed PLA/PCL composites as a function of PCL contents are shown by the blue line in Fig. 4b. The T_m of the PLA/PCL composites stays almost the same at around 167 °C, indicating the good thermal stability against high temperatures.

Figs. 4c and 4d show the DMA results of pure PLA and $PLA_{0.80}/PCL_{0.20}$ composite made by 3D printing. As demonstrated in Fig. 4c, the storage modulus of pure PLA at 0 °C is 3283 MPa, which is higher than that of $PLA_{0.80}/PCL_{0.20}$ (1438 MPa), indicating that the PLA/PCL composites with smaller PCL content can store more stresses when they are deformed, and can recover their initial shapes more easily

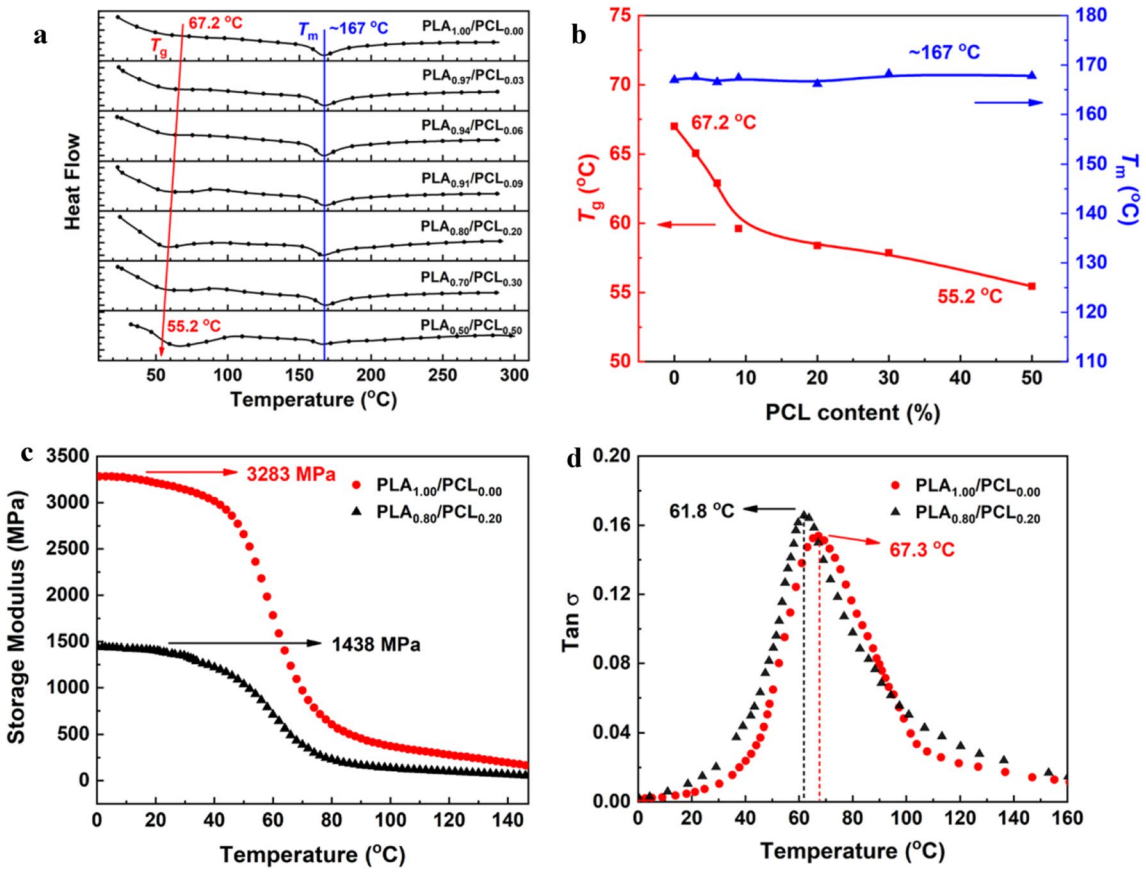

Fig. 4 **a** DSC scans of the 4D-printed PLA/PCL composites. **b** T_g and T_m of the 4D-printed PLA/PCL composites as a function of the PCL content. **c** The storage modulus and **d** tanσ of $PLA_{1.00}/PCL_{0.00}$ and $PLA_{0.80}/PCL_{0.20}$ at different temperatures

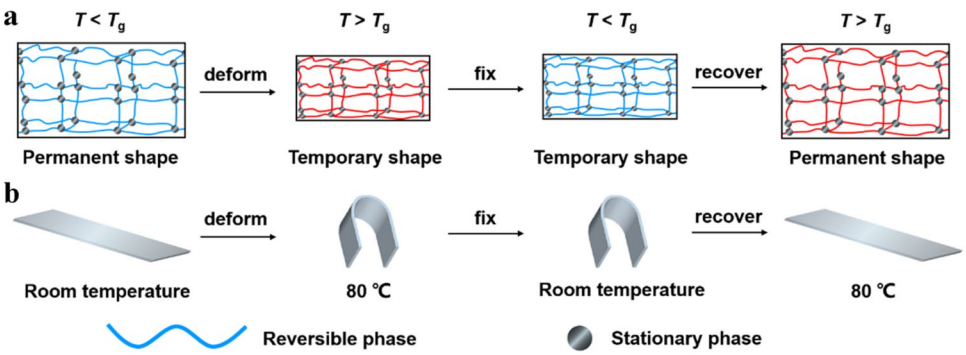

Fig. 5 Schematic diagrams of **a** the shape memory mechanism of the 4D-printed PLA/PCL composite samples and **b** the shape memory process of the 4D-printed PLA/PCL composite samples

when the stresses are released. The peak temperatures of the loss factors (tanσ) in Fig. 4d reflect the T_g of the materials, which were determined to be 67.3 °C and 61.8 °C for pure PLA and $PLA_{0.80}/PCL_{0.20}$, respectively, which corresponds well with the DSC test results. Therefore, the differences in the mechanical properties and T_g values for these 4D-printed PLA/PCL composites can be used to generate different shape memory behaviors under the same heating conditions.

Shape memory behaviors

The shape memory effect of SMPs originates from two separate domains in the polymer, i.e., a crystalline domain as a stationary phase, and an amorphous domain as a reversible phase [25, 26]. The mechanism of shape memory effect for the 4D-printed PLA/PCL composites is shown in Fig. 5. It can be seen that the non-crosslinked PCL has no shape

memory effect and thus the shape memory behavior of the PLA/PCL composites is mainly attributed to PLA. As illustrated in Fig. 5, the flexible polymer chains in PLA act as the reversible phase, and the crosslinked spots in PLA act as the stationary phase. When the materials are heated above T_g, the movements of the flexible polymer chains intensify, making it easy for the samples to deform to any shape under external applied forces. On the microscale, this consists the change of molecular conformations of PLA chains, which is reflected in the change of sample shapes on the macroscale. Such temporary shapes can be fixed well by cooling down the samples below T_g. In this case, the crosslinked stationary phases play an important role in fixing the temporary shape. When the samples are heated above T_g again, the flexible PLA polymer chains relax and return to the original molecular conformations, leading to the release of stored stress and the recovery of the shape to the printed permanent shape.

With the addition of PCL to the PLA matrix, the 4D-printed PLA/PCL composites exhibit decreased T_g, which is beneficial for applications in the biomedical field. The shape memory behaviors of the 4D-printed PLA/PCL composites were first studied by fixing them to a U-shape, as shown in Fig. 6a. The shape fixation rate (R_f) and the shape recovery rate (R_r) were calculated according to Fig. 6b and Eqs. (A1) and (A2) (see Appendix). The shape recovery processes of the 4D-printed PLA/PCL composites with different PCL contents were one-way shape recovery effects, which were recorded as shown in Fig. 6c. First, the sheet-like 4D-printed PLA/PCL composites were transferred into a water bath under temperature above their T_g; after applying external forces and cooling them down, the samples were fixed into the temporary U-shape. As summarized in Table 2, the R_f values of samples rise with increasing PCL content, and are all above 95%. Second, the 4D-printed PLA/PCL composites with temporary shapes were put into the hot water bath again to automatically recover their original sheet-like shape. As demonstrated in Fig. 6c, the samples with U-shape can recover their original shapes within 1.2 s, indicating their fast response to temperature. In addition, the R_r value of the samples is above 99.7%, demonstrating their excellent shape recovery performance.

In order to further investigate the shape memory properties of the 4D-printed PLA/PCL composites, a complicated helical shape was applied as the temporary shape. As shown in Fig. 7c, all samples can fix the helical shape well with a shape fixation rate above 95% (Table A2, see Appendix), which can be calculated using the diameters of the helical shapes (Fig. 7b) according to Eq. (A3) in Appendix. Despite the complicated temporary shape, the samples can quickly recover their permanent shapes upon heating while featuring high shape recovery rates above 92%, which are defined as the comparison between the original shape index and the recovery shape index (Fig. 7b and Eq. (A4) (see Appendix)). In the same way as those with U-shape, the 4D-printed PLA/PCL composites with helical temporary shape show a fast shape recovery process and shape recovery times that vary with PCL content. With the increase in the latter, the shape

Table 2 Summary of the shape memory properties of the 4D-printed PLA/PCL composites

Sample	R_f (%)	R_r (%)	Shape recovery time (s)
$PLA_{1.00}/PCL_{0.00}$	95.12	99.9	0.4
$PLA_{0.97}/PCL_{0.03}$	95.63	99.8	0.6
$PLA_{0.94}/PCL_{0.06}$	96.24	99.9	0.8
$PLA_{0.91}/PCL_{0.09}$	96.38	99.9	0.8
$PLA_{0.90}/PCL_{0.10}$	96.16	99.8	0.9
$PLA_{0.80}/PCL_{0.20}$	97.05	99.7	1
$PLA_{0.70}/PCL_{0.30}$	97.84	99.9	1
$PLA_{0.50}/PCL_{0.50}$	97.21	99.9	1.2

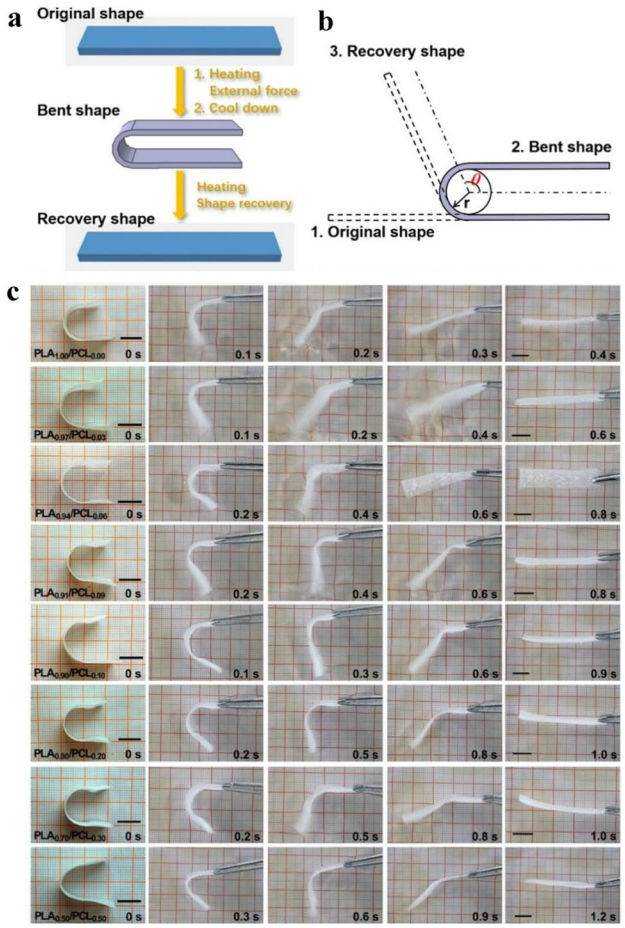

Fig. 6 **a**, **b** Schematic of the shape memory process of the 4D-printed PLA/PCL composites with a temporary "U" shape. **c** Shape recovery process of the 4D-printed PLA/PCL composites with the temporary shape fixed to a U-shape. Scale bar: 1 cm

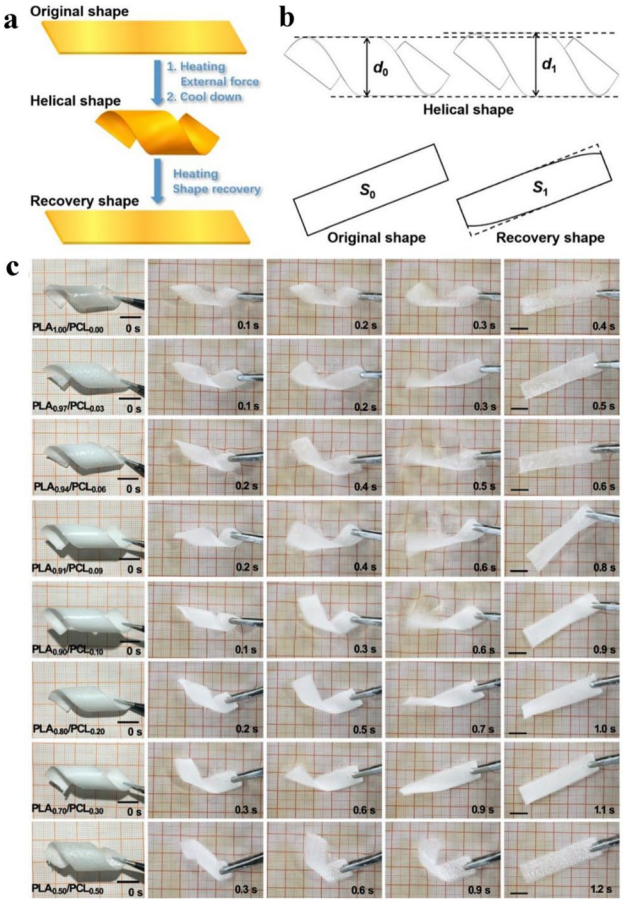

Fig. 7 **a**, **b** Schematic of shape memory process for the 4D-printed PLA/PCL composites with a helical temporary shape. **c** Shape recovery process of the 4D-printed PLA/PCL composites with the temporary shape fixed to a helical shape. Scale bar: 1 cm

recovery time increases slightly from 0.4 to 1.2 s. As a result of PCL addition, although the deformation temperatures decrease remarkably (which can facilitate the shape recovery process), the modulus reduction can reduce the stress stored inside the materials when fixed into a temporary shape, which can lead to a slower shape recovery process. Accordingly, based on the 4D-printed PLA/PCL composites in this work, the differences in shape recovery time can provide a great opportunity to realize controllable sequential deformation processes.

Bio-design application examples

A double-layer bionic flower was assembled by two separately printed PLA/PCL layers with different PCL contents to simulate the one-way opening process of a chrysanthemum (Fig. 8a). As shown in the inset of Fig. 8a, the permanent shape of the bionic flower was initially "open," with the top layer printed by $PLA_{0.50}/PCL_{0.50}$ and the bottom layer printed by $PLA_{0.90}/PCL_{0.10}$. The bionic flower was then fixed to a "closed" state as shown in Fig. 8b, and put into an 80 °C water bath. The sequential petal opening process was recorded as indicated in Figs. 8c–8f. Since $PLA_{0.90}/PCL_{0.10}$ has a shorter shape recovery time and a faster response to temperature compared to $PLA_{0.50}/PCL_{0.50}$, the bottom blue petals open at a faster speed, whereas the opening of the top white petals is a more gradual process. The behaviors of this bionic flower demonstrate the controllable sequential deformation by using 4D-printed PLA/PCL composites with different PLA: PCL ratios, indicating their potential application in the fields of biomedical devices.

The study of shape memory effects indicates that the 4D-printed PLA/PCL samples with higher PCL concentrations show a slower shape recovery process and longer shape recovery time. Therefore, a drug release device as a potential

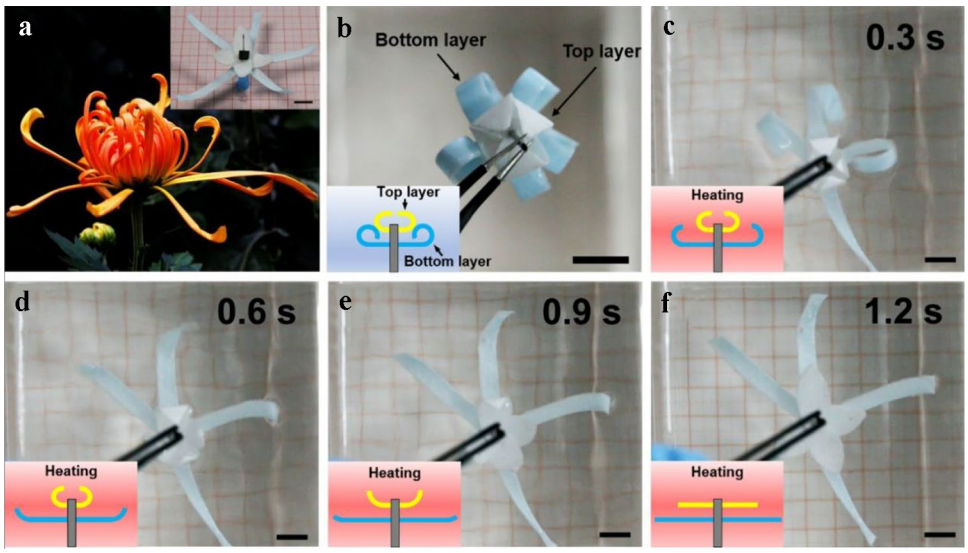

Fig. 8 **a** Photograph of a 4D-printed chrysanthemum. The inset is the initial shape of the double-layer bionic flower with "open" state. **b** The double-layer bionic flower with "closed" temporary state. The bottom layer (blue) was printed by $PLA_{0.90}/PCL_{0.10}$, and the top layer (white) was printed by $PLA_{0.50}/PCL_{0.50}$. **c**–**f** The controllable sequential petal opening processes of the bionic flower. Scale bar: 1 cm

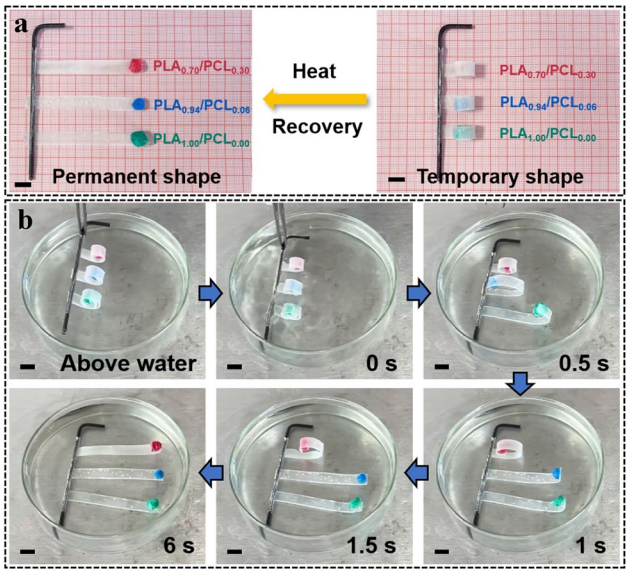

Fig. 9 **a** A drug release device based on $PLA_{1.00}/PCL_{0.00}$ (green pellet), $PLA_{0.94}/PCL_{0.06}$ (blue pellet), and $PLA_{0.70}/PCL_{0.30}$ (red pellet). The photographs show the device with "released" permanent state and "closed" temporary state. **b** The sequential drug release processes of the different pellets with different times. Scale bar: 1 cm

biomedical application was fabricated based on three different PLA/PCL samples to realize sequential drug release. As shown in Fig. 9a, green, blue, and red pellets were attached to one end of the $PLA_{1.00}/PCL_{0.00}$, $PLA_{0.94}/PCL_{0.06}$, and $PLA_{0.70}/PCL_{0.30}$ stripes (70 mm × 8 mm × 0.5 mm), respectively. Next, the 4D-printed PLA/PCL stripes were rolled to the temporary shapes with the pellets kept inside. The drug release processes of the device are shown in Fig. 9b. The green pellet was first released within 0.5 s, as the $PLA_{1.00}/PCL_{0.00}$ stripe had the fastest shape memory effect. The blue pellet was subsequently released within 1 s, and the red pellet was finally released after 6 s. The sequential drug release process is attributed to the different shape recovery time of 4D-printed PLA/PCL samples with different PLA: PCL ratios, and the order of the released drugs is in good agreement with the shape recovery order recorded in Table 2. Additionally, to evaluate the maximum weight of the pellets that can be lifted by the drug release device, the shape recovery forces of the PLA/PCL composite strips were recorded on a force transducer (Fig. A3a, see Appendix). As depicted in Fig. A3b in Appendix, the maximum forces of $PLA_{1.00}/PCL_{0.00}$, $PLA_{0.94}/PCL_{0.06}$, and $PLA_{0.70}/PCL_{0.30}$ stripes were 74, 46, and 21 mN, respectively, corresponding to 7.55, 4.69, and 2.14 g, respectively. These results indicate that PLA/PCL composites with smaller PCL contents generate larger shape recovery forces, which is also accordant with the DMA test in Fig. 4c. Moreover, since both PLA and PCL are biodegradable and biocompatible materials, it is feasible to use PLA/PCL composite devices in biomedical environments.

Conclusions

In the present study, DW 3D printing was applied to fabricate a series of PLA/PCL composites, which showed controllable sequential shape memory behaviors. The introduction of PCL to the PLA matrix can affect the properties of the composite material in several ways: (1) the T_g of the 4D-printed PLA/PCL composites decreases with increasing PCL content from 67.2 °C for pure PLA down to 55.2 °C for $PLA_{0.50}/PCL_{0.50}$; (2) a small proportion of PCL ($\leq 10\%$) can raise the maximum strain of PLA, thereby making the material soft and flexible; (3) the shape recovery time decreases with increasing PCL content. Based on these 4D-printed PLA/PCL composites, a double-layer bionic flower and a drug release device were fabricated to simulate sequential petal opening and sequential drug releasing effects, respectively, indicating the potential applications of 4D-printed PLA/PCL composites in the field of smart actuators, biomedical devices, and so on.

Appendix

DW 3D printer

The homemade DW 3D printer is illustrated in Fig. A1. The printing head of the DW printer is a syringe with nozzle diameter of 640 μm. The printing route is controlled by a three-dimensional moving stage, and the printing platform is a Teflon plate with a smooth surface.

Material preparation

The material components of the printing ink are shown in Table A1. The PLA/PCL composites are named as PLA_{1-x}/PCL_x, where x is the mass ratio of PCL in PLA and PCL, respectively. The PLA/PCL powder and nano-silica

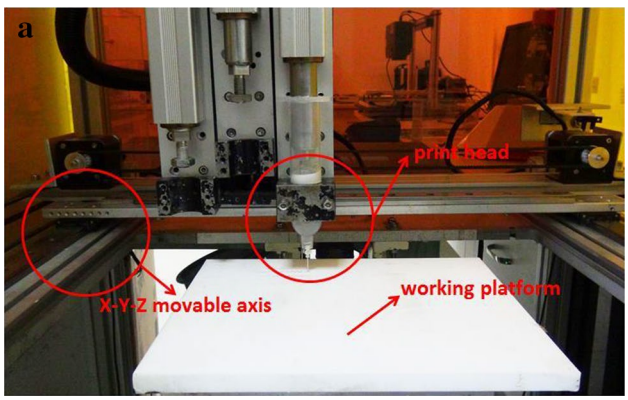

Fig. A1 Photograph of the homemade DW 3D printer

Table A1 Material components of the PLA/PCL composite ink for 4D printing

Sample	PLA (g)	PCL (g)	CH_2Cl_2 (g)	Nano-silica (mg)
$PLA_{1.00}/PCL_{0.00}$	5.00	0.00	15	2.5
$PLA_{0.97}/PCL_{0.03}$	4.85	0.15	15	2.5
$PLA_{0.94}/PCL_{0.06}$	4.70	0.30	15	2.5
$PLA_{0.91}/PCL_{0.09}$	4.65	0.35	15	2.5
$PLA_{0.90}/PCL_{0.10}$	4.50	0.50	15	2.5
$PLA_{0.80}/PCL_{0.20}$	4.00	1.00	15	2.5
$PLA_{0.70}/PCL_{0.30}$	3.50	1.50	15	2.5
$PLA_{0.50}/PCL_{0.50}$	2.50	2.50	15	2.5

were added to CH_2Cl_2 solvent with a mass ratio of PLA/PCL:nano-silica:CH_2Cl_2 = 1:0.0005:3.

Molding method for PLA sample preparation

The schematic of molding is depicted in Fig. A2. For pure PLA samples, the solution was prepared according to the material content of $PLA_{1.00}/PCL_{0.00}$. The molding method includes the following steps: (1) pour the PLA solution into a Teflon mold and scrape the top of the solution to be flat; (2) shake the mold to get rid of air bubbles; (3) dry the PLA solution at room temperature for 36 h; (4) peel the PLA samples off the Teflon mold.

Shape fixation/recovery rate of U-shape

The shape fixation rate (R_f) is calculated according to the following equation:

$$R_f = \frac{180° - \theta_1}{180° - \theta_0} \times 100\%. \tag{A1}$$

The shape recovery rate (R_r) is calculated according to the following equation:

Table A2 Summary of the shape memory properties of the 4D-printed PLA/PCL composites when fixed to a helical shape

Sample	R_f (%)	R_r (%)	Shape recovery time (s)
$PLA_{1.00}/PCL_{0.00}$	98.31	98.7	0.4
$PLA_{0.97}/PCL_{0.03}$	97.26	98.3	0.5
$PLA_{0.94}/PCL_{0.06}$	97.21	96.7	0.6
$PLA_{0.91}/PCL_{0.09}$	97.36	92.3	0.8
$PLA_{0.90}/PCL_{0.10}$	96.66	97.8	0.9
$PLA_{0.80}/PCL_{0.20}$	96.07	93.4	1
$PLA_{0.70}/PCL_{0.30}$	96.23	99.1	1.1
$PLA_{0.50}/PCL_{0.50}$	95.48	99.8	1.2

$$R_r = \frac{\theta_2 - \theta_1}{180° - \theta_1} \times 100\%, \tag{A2}$$

where θ_0 represents the angle with external force once the sample has been fixed to the temporary U-shape, θ_1 represents the angle after cooling down the sample and releasing the external force, and θ_2 represents the angle after heating the sample up again and recovering it to the original shape.

Shape fixation/recovery rate of helical shape

The shape fixation rate (R_f) is calculated according to the following equation:

$$R_f = \left(1 - \frac{d_1 - d_0}{d_0}\right) \times 100\%, \tag{A3}$$

where d_0 represents the outer diameter of the helical shape with external force once the sample has been fixed to the temporary helical shape, and d_1 represents the outer diameter after cooling down the sample and releasing the external force.

The shape recovery rate (R_r) is calculated according to the following equation:

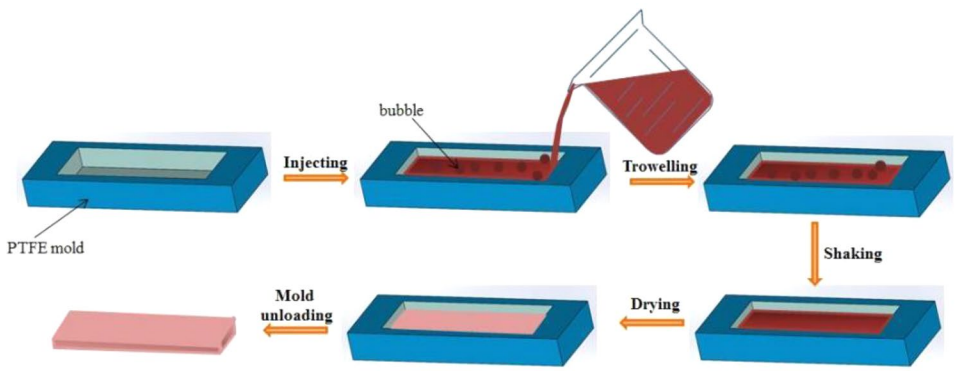

Fig. A2 Schematic of the fabrication process of molding

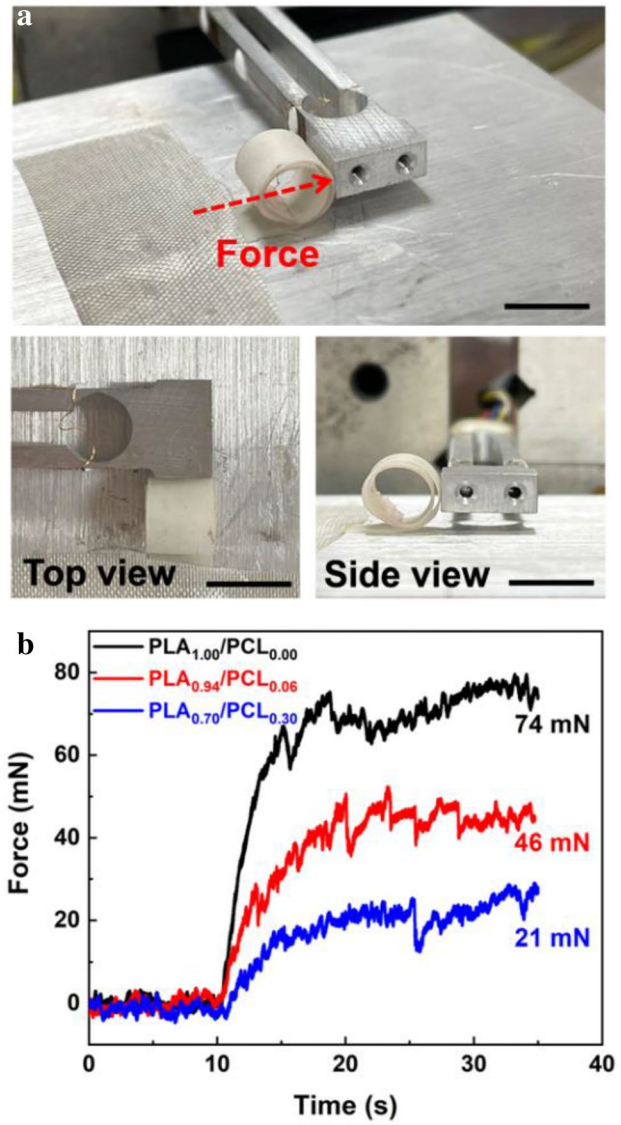

Fig. A3 **a** Photographs of force measurement recorded using a 500-mN force transducer. **b** Shape recovery forces of the drug release devices based on $PLA_{1.00}/PCL_{0.00}$, $PLA_{0.94}/PCL_{0.06}$, and $PLA_{0.70}/PCL_{0.30}$. Scale bar: 1 cm

$$R_r = \frac{S_1}{S_0} \times 100\%, \tag{A4}$$

where S_0 represents the original rectangle area of the sheet-like sample, and S_1 represents the projected area of the recovered sample.

Shape memory properties when fixed to a helical shape

The shape memory properties, including the shape fixation rate, shape recovery rate, and shape recovery time of the 4D-printed PLA/PCL samples fixed to a helical shape, are summarized in Table A2.

Force measurement of drug release devices

The force measurement was performed on a one-dimensional force transducer (500 mN, NBIT, Nanjing, China). As shown in Fig. A3a, the samples with a temporary "closed" state were placed on a hot plate 2 mm away from the force transducer, with one end pasted on the hot plate. When the samples were heated above T_g, they tended to recover to their original "open" state and then touch the force transducer, which could record the forces generated by the samples. The measured forces shown in Fig. A3b can be transferred into the mass of the pellets according to the equation of $F = mg$, where F denotes the force, m represents the mass, and g is 9.8 N/kg.

Acknowledgements This work was supported by the Project of National Key Research and Development Program of China (Nos. 2018YFB1105100 and 2018YFC2001300), the National Natural Science Foundation of China (Nos. 5167050531, 51822504, 91848204, 91948302, and 52021003), the Key Scientific and Technological Project of Jilin Province (No. 20180201051GX), the Program for JLU Science and Technology Innovative Research Team (No. 2017TD-04), and the Scientific Research Project of Education Department of Jilin Province (No. JJKH20211084KJ).

Author contributions SQM and ZYJ performed the experiments and wrote the draft of manuscript; MW and LZ analyzed the data; YHL and LR proposed the project and critical comments on the writing of the manuscript; ZHZ and LQR provided some additional suggestions on experiments. SQM, ZYJ, MW, LZ, YHL, ZHZ, LR, and LQR contributed to the general discussion.

Declarations

Conflict of interest The authors declare that they have no conflict of interest.

Ethical approval This study does not contain any studies with human or animal subjects performed by any of the authors.

References

1. Zhou C, Chen Y, Yang Z et al (2013) Digital material fabrication using mask-image-projection-based stereolithography. Rapid Prototyp J 19(3):153–165. https://doi.org/10.1108/13552541311312148
2. Khoo ZX, Teoh JEM, Liu Y et al (2015) 3D printing of smart materials: a review on recent progresses in 4D printing. Virtual Phys Prototyp 10(3):103–122. https://doi.org/10.1080/17452759.2015.1097054
3. Wei H, Wan X, Liu Y et al (2018) 4D printing of shape memory polymers: research status and application prospects. Sci Sin Technol 48(1):2–16. https://doi.org/10.1002/adfm.202100257
4. Liu TZ, Zhou TY, Yao YT et al (2017) Stimulus methods of multi-functional shape memory polymer nanocomposites: a review.

Compos Part A Appl Sci Manuf 100:20–30. https://doi.org/10.1016/j.compositesa.2017.04.022
5. Mu T, Liu L, Lan X et al (2018) Shape memory polymers for composites. Compos Sci Technol 160:169–198. https://doi.org/10.1016/j.compscitech.2018.03.018
6. Wu JJ, Huang LM, Zhao Q et al (2018) 4D printing: history and recent progress. Chin J Polym Sci 36(5):563–575. https://doi.org/10.1007/s10118-018-2089-8
7. Senatov FS, Niaza KV, Zadorozhnyy MY et al (2016) Mechanical properties and shape memory effect of 3D-printed PLA-based porous scaffolds. J Mech Behav Biomed 57:139–148. https://doi.org/10.1016/j.jmbbm.2015.11.036
8. Zhang X, Geven MA, Grijpma DW et al (2017) Tunable and processable shape memory composites based on degradable polymers. Polymer 122:323–331. https://doi.org/10.1016/j.polymer.2017.06.066
9. Lipton JI, Cutler M, Nigl F et al (2015) Additive manufacturing for the food industry. Trends Food Sci Technol 43(1):114–123. https://doi.org/10.1016/j.tifs.2015.02.004
10. Patra S, Young V (2016) A review of 3D printing techniques and the future in biofabrication of bioprinted tissue. Cell Biochem Biophys 74(2):93–98. https://doi.org/10.1007/s12013-016-0730-0
11. Wendel B, Rietzel D, Kühnlein F et al (2018) Additive processing of polymers. Macromol Mater Eng 293(10):799–809. https://doi.org/10.1002/mame.200800121
12. Zocca A, Colombo P, Gomes CM et al (2015) Additive manufacturing of ceramics: issues, potentialities, and opportunities. J Am Ceram Soc 98(7):1983–2001. https://doi.org/10.1111/jace.13700
13. Ho CMB, Ng SH, Yoon YJ (2015) A review on 3D printed bioimplants. Int J Precis Eng Manuf 16(5):1035–1046. https://doi.org/10.1007/s12541-015-0134-x
14. Guo N, Leu MC (2013) Additive manufacturing: technology, applications and research needs. Front Mech Eng 8(3):215–243. https://doi.org/10.1007/s11465-013-0248-8
15. Quan ZZ, Wu A, Keefe M et al (2015) Additive manufacturing of multi-directional preforms for composites: opportunities and challenges. Mater Today 18(9):503–512. https://doi.org/10.1016/j.mattod.2015.05.001
16. Ngo TD, Kashani A, Imbalzano G et al (2018) Additive manufacturing (3D printing): a review of materials, methods, applications and challenges. Compos Part B Eng 143:172–196. https://doi.org/10.1016/j.compositesb.2018.02.012
17. Momeni F, Seyed MMHN, Liu X et al (2017) A review of 4D printing. Mater Des 122:42–79. https://doi.org/10.1016/j.matdes.2017.02.068
18. Ren LQ, Li BQ, Song ZY et al (2019) Bioinspired fiber-regulated composite with tunable permanent shape and shape memory properties via 3d magnetic printing. Compos Part B 164:458–466. https://doi.org/10.1016/j.compositesb.2019.01.061
19. Ren LQ, Zhou XL, Liu QP et al (2018) 3D magnetic printing of bio-inspired composites with tunable mechanical properties. J Mater Sci 53(20):14274–14286. https://doi.org/10.1007/s10853-018-2447-5
20. Ma SQ, Zhang YP, Wang M et al (2020) Recent progress in 4D printing of stimuli-responsive polymeric materials. Sci China Technol Sci 63(4):532–544. https://doi.org/10.1007/s11431-019-1443-1
21. Ma S, Zhang Y, Liang Y et al (2020) High-performance ionic-polymer-metal composite: toward large-deformation fast-response artificial muscles. Adv Funct Mater 30(7):1908508. https://doi.org/10.1002/adfm.201908508
22. Yu K, Ritchie A, Mao YQ et al (2015) Controlled sequential shape changing components by 3D printing of shape memory polymer multimaterials. Procedia IUTAM 12:193–203. https://doi.org/10.1016/j.piutam.2014.12.021
23. Li XJ, Pan Y, Deng JN et al (2017) Multiscale-structuring of rapid response shape memory polymers based on self-assembly reverse micelles. React Funct Polym 121:1–7. https://doi.org/10.1016/j.reactfunctpolym.2017.10.002
24. Maurath J, Willenbacher N (2017) 3D printing of open-porous cellular ceramics with high specific strength. J Eur Ceram Soc 37(15):4833–4842. https://doi.org/10.1016/j.jeurceramsoc.2017.06.001
25. Sobota M, Jurczyk S, Kwiecien M et al (2017) Crystallinity as a tunable switch of poly(L-lactide) shape memory effects. J Mech Behav Biomed 66:144–151. https://doi.org/10.1016/j.jmbbm.2016.11.009
26. Zhang L, Lin Z, Zhou Q et al (2020) PEEK modified PLA shape memory blends: towards enhanced mechanical and deformation properties. Front Mater Sci 14(2):177–187. https://doi.org/10.1007/s11706-020-0502-z